CHARACTERIZING THE EFFLUENCE NEAR WAIKĪKĪ, HAWAIʻI WITH A COUPLED BIOPHYSICAL MODEL

A THESIS SUBMITTED TO THE GRADUATE DIVISION OF THE UNIVERSITY OF HAWAIʻI AT MĀNOA IN PARTIAL FULFILLMENT OF THE REQUIREMENTS FOR THE DEGREE OF

MASTER OF SCIENCE

IN

OCEANOGRAPHY

MAY 2012

By

Abby Johnson

Thesis Committee:

Brian S. Powell, Chairperson
Mark A. Merrifield
Grieg F. Steward

Acknowledgments

I would like to thank my advisor, Dr. Brian Powell, for his support, guidance and patience throughout my time here at the University of Hawaii. I would like to thank Dr. Mark Merrifield and Dr. Grieg Steward for serving on my thesis committee and for sharing their expertise. Thank you to the members of Brian's lab: Marcia Hsu, Ivica Janekovic, Dax Matthews, Becky Baltes, and Colette Kerry for all of your time and help.

I would like to thank those who have supplied me with the observational data to complete this project: Heather Jeppesen from USGS, Jennifer Patterson from HIOOS, Mark Ericksen and Andrew Rocheleau from Sea Engineering, Y. Chen, Pat Caldwell and Robert E. Jensen.

This would not have been possible without the support and encouragement from my family. And last, but not least, thank you to all of my friends that were there for me along the way especially: Lindsey Shank, John Casey, KR MacDonald, Kristen Fogaren, Jerome Aucan, Cameron McNaughton, Mitchell Pinkerton, Adam Jenkins, CJ Bradley and Noelani Goldstein.

Abstract

Aperiodic discharge from the Ala Wai Canal near Waikiki, Hawaii is contaminated with naturally occurring harmful bacteria. We use a coupled hydrodynamic and biological model to examine how tides, wind, surface waves, and light affect the fate of the effluent plume. The freshwater plume is constrained to the surface and advected by the ambient and tidal flow. Winds overcome the background advection and keep the plume from the Waikiki beaches and mix the plume downward. Surface waves also mix the plume water and keep the plume near-shore. We find that the plume does not extend offshore in the presence of winds or waves. Using *Enterococcus* spp. as the bacterial agent, we find that residency is increased when mixed deeper away from the light. Comparing predicted *Enterococcus* spp. with in-situ samples for five distinct outflow events, we find that the model well captures the observed bacteria when the Ala Wai is the source of discharge. The results show that such a system may be valuable to predicting times and locations for harmful effluent plumes near the Ala Wai Canal.

Table of Contents

List of Tables

List of Figures

1. Introduction

Freshwater plumes are a source of sediments, nutrients, and pollutants into the ocean that affect near-shore coastal waters (Masse and Murthy, 1992). The near-shore physical forcing (e.g., ambient flow, wind, tides, and waves) play an important role in characterizing the dynamics of these outflows such that understanding the local physics is crucial to each outflow. Numerous studies have been conducted to better understand how outflows disperse upon entering the coastal ocean (Garvine, 1995; Hickey et al., 1998; Orton and Jay, 2005). Modeling studies (O'Donnell, 1990; Wiseman and Garvine 1995; Berdeal et al., 2002; Choi and Wilkin, 2007) have helped to parameterize the effects of wind, tides, and bathymetry on the evolution of persistent large-scale plumes, but the effects of wave forcing and light variability remain poorly constrained.

Numerical simulations have been used to characterize freshwater coastal plumes, but the focus has been on high-volume outflows with large Kelvin numbers, K (see Garvine 1987, 1995; O'Donnell, 1990; Wiseman and Garvine, 1995). Plumes with $K \geq 1$ are affected by rotation due to the Coriolis force, while those with a small K (< 1) are most influenced by the motion of the ambient coastal water (Garvine, 1987 and 1995; O'Donnell, 1990).

Tidal forcing strongly influences both small and large-scale coastal discharges. It affects the small-scale discharge of the Connecticut River by moving the plume to the east of the river mouth on an ebb tide and to the west on a flood tide (Whitney and Garvine, 2006). Using a numerical model, Guo and Valle-Levinson (2007) analyzed tidal effects on an outflow plume in Chesapeake Bay and concluded that a bottom-advected plume occurred due to tidal forcing whereas a surface-advected plume developed without tidal forcing. For the high-volume river outflow of the Columbia River, plume mixing was strongest near the tidal plume front, which exchanges nutrients and sediments (Orton and Jay, 2005). Although some tidal forcing effects on freshwater plumes have been considered (Wiseman and Garvine, 1995; Orton and Jay, 2005; Whitney and Garvine, 2006; Guo and Valle-Levinson, 2007), the majority of studies have focused on the effects of wind forcing on plumes with large K values.

Wind forcing has the potential to influence the advection, mixing, and transport of river plumes. Numerical modeling studies have been carried out to determine the effect

of wind forcing on large-scale discharges like the Columbia River and the Hudson River. Choi and Wilkin (2007) showed that wind forcing affected the amount of discharge and the trajectory of the surface-advected Hudson River plume. For a high-discharge event without wind forcing, the plume formed a large recirculating bulge of freshwater outside the river mouth. Southward winds advected the plume to the south and northward wind advected the plume offshore and along the Long Island coast. Eastward winds increased the freshwater transport from the mouth of the river whereas westward wind caused a decrease. Hickey et al. (1998) and Berdeal et al. (2002) found that the Columbia River plume responded to wind forcing within hours and moved offshore with southward, upwelling winds that tend to occur during the summer and moved onshore during northward, downwelling winds that occur in the winter. Downwelling-favorable winds can also create vertical mixing and a deepening of a freshwater plume (Pullen and Allen, 2000).

All of these studies were on systems with significant, regular outflow. In this study, we examined effluent outflow from the Ala Wai Canal, a small freshwater plume associated with an artificial estuary located two kilometers northwest of the beaches at Waikiki in Honolulu, Hawaii. Since the canal was built, its water quality has deteriorated such that it can be a public health risk (Venzon, 2007) and has been found to be a source of fecal contamination to nearby beaches. Due to infection risks associated with outflow events, a predictive tool of plume evolution would be desirable for civil planning purposes and could improve assessment risks to beachgoers. Notably, a causal correlation between *Enterococcus* spp. abundance, inferred from extinction culturing, in near-shore waters and episodic rainfall events has been established (Hamilton et al., 1995; Connolly et al., 1999); however, a mechanistic understanding of the specific contribution of the outflow from the Ala Wai Canal is lacking. We aim to examine aperiodic effluent outflows from a small canal into a reef-protected surf zone and determine what controls the fate of the harmful bacteria. We present the use of a biological model of *Enterococcus* spp. nested in a high-resolution numerical circulation model to examine the effects of physical forcing (ambient flow, wind, tides, and waves) on a low-volume freshwater plume.

2. Methods

2.1 *ROMS*

We use the Regional Ocean Modeling System (ROMS) model to characterize the circulation of Mamala Bay along the south coast of Oahu, and the effects on runoff events from the Ala Wai Canal. ROMS is a high-resolution, hydrostatic, free-surface, terrain-following vertical coordinate oceanic model built using the Boussinesq, hydrostatic momentum, and mass balance equations. The hydrostatic primitive equation for momentum is solved using a split-explicit time-stepping scheme and coupling between barotropic and baroclinic modes (Shchepetkin and McWilliams, 2004). The resolution of the model grid is variable, ranging from 66 m cross-shore resolution at the shore to 575 m in the deep water offshore. It covers the south shore of Oahu, extending from Diamond Head to Barber's Point and includes the Ala Wai Canal, Keehi Lagoon, and entrance to Pearl Harbor and extends approximately 15.5 km offshore as shown in Figure 1. The model contains 20 vertical sigma layers.

The grid used for this study is nested within two other model grids. The middle grid comprises all of the island of Oahu as well as the Kaiwi Channel and the western portion of Molokai. The middle grid is nested within the ROMS outer-most grid, which is comprised of all the major Hawaiian Islands. The Navy Coastal Ocean Model (NCOM) provides a daily global ocean forecast with $1/8^{o}$ resolution which is used to generate boundary conditions for the outer-most grid. The boundary conditions for the model used in this study are provided by the middle grid.

For each outflow event, the model was integrated for twelve different configurations in order to determine the effects of the physical forcing as listed in Table 1. Each experiment spans a two week time period surrounding the event using all configurations. The outer-model grids are integrated with all physical forcing except waves to provide boundary conditions for the grid in this study. For experiments without tidal forcing, boundary conditions are detided to eliminate barotropic and baroclinic tides. This ensures consistent low-frequency dynamics between all configurations.

All experiments include the ambient flow of Mamala Bay, which is provided by the outer-model. The dominant flow around the Hawaiian island chain is comprised of the North Equatorial Current (NEC), North Hawaiian Ridge Current (NHRC), Hawaiian

Lee Current (HLC), and the Hawaiian Lee Counter Current (HLCC). The NEC flows from east to west and forms two branches upon encountering the island of Hawaii. Due to wind stress patterns the HLCC is formed and flows west to east behind the island of Hawaii. The HLCC turns and flows along the southern side of the island chain forming the HLC. The HLC produces onshore bifurcating flow into Mamala Bay, linking circulation in Mamala Bay with the canonical flow pattern around the Hawaiian island chain.

We compare an acoustic Doppler current profiler (ADCP) deployed 2.5 km offshore of Sand Island (see Fig. 1) during 2007. Model and observed velocities were oriented into alongshore and cross-shore directions and the time-mean at each depth were compared (Figure 2). The modeled alongshore currents were slightly stronger than the observed currents with both showing a velocity inversion at approximately 45 m suggesting a two-layer flow. For cross-shore currents above 25 m, the ADCP currents were slightly stronger, while model currents were slightly stronger below 25 m. Root mean square error (RMS) values ranged from 0.43 – 0.84 cm s^{-1} for alongshore currents and RMS values ranged from 0.09 – 0.76 cm s^{-1} for cross-shore currents. Along with errors less than 1 cm s^{-1}, the model captured the amplitude and two-layer structure of the mean flow such that we can examine how variations about the mean influence the plume.

Atmospheric forcing for the model is provided by a locally run regional weather research and forecasting (WRF) model with 1.5 km resolution. The ocean model is forced by the atmospheric variables: surface air temperature, rainfall rate, surface air pressure, surface air relative humidity, surface winds at 10 m, net longwave radiation flux, and solar shortwave radiation flux via the Coupled Ocean-Atmosphere Response Experiment (COARE) flux algorithm (Fairall et al., 1996). Trade winds blow from the northeast to the southwest and are the dominant winds for the Hawaiian Islands. From October to April it is common for the Trade winds to weaken and storm winds blow from the southerly direction known as Kona winds. To examine the role of the winds, the wind forcing is set to zero for some experiments (while maintaining the heat and mass fluxes).

Tidal forcing, which includes barotropic and baroclinic tides, is imposed through the boundary conditions to examine the impact on the plume. The Oregon State

University TOPEX/POSEIDON Global Inverse Solution (TPXO) provides barotropic tidal forcing to the outer-most model (Egbert et al., 1994). Conversion from the barotropic to baroclinic tides occurs along the steep ridges of the nested model. The alongshore coastal currents in Mamala Bay are dominated by the tides, primarily the semidiurnal M_2 constituent. The semidiurnal tide propagates from the northeast to the southwest as it approaches Oahu. The Hawaiian Ridge refracts the wave causing it to split at Oahu, propagating around the east and west sides of the island to merge within Mamala Bay (Hamilton et al., 1995). Due to this merging, there are strong alongshore tidal velocities at the headlands and small cross-shore velocities within the bay. More than 70% of the near-shore current variance at the Ala Wai Canal is due to the tides, and the majority (97.5%) of that variance is in the alongshore direction. During ebb tide the flow is to the east towards Waikiki beaches, and during flood tide the flow is to the west towards Ala Moana Beach Park.

Surface wave forcing is included in some experiments to examine its effects on the plume. Wave data was obtained from the U.S. Army Corps of Engineers (USACE) Wave Information Studies that estimates past wave conditions using a computer model with observed winds to hindcast wave conditions. The average and maximum south swell conditions were taken at the closest synthetic buoy located southwest of the island of Oahu. A wind-wave model (WWM) was used to create a spectral representation of these wave conditions along the south shore of Oahu. The significant wave height for the average south swell conditions was 1.34 m with a period of 13.28 s. For maximum south swell conditions the significant wave height was 1.67 m at a period of 13.85 s. Both swell conditions propagated from 190^o (nearly from South). The significant wave height, period, wavelength, and direction parameters generated were used as wave forcing of the ROMS model for the five outflow events.

In order to simulate outflow events, the model domain contains an Ala Wai Canal of similar length, width, and depth. The total volume of the model Ala Wai Canal is similar to the estimated volume generated from data collected from multibeam bathymetry data obtained from the Hawaii Ocean Observing System. A time series of Manoa Stream discharge data was obtained from the United States Geological Survey (USGS) at the Manoa-Palolo drainage canal. The Manoa-Palolo drainage canal makes up

approximately 70% of the total freshwater input to the Ala Wai Canal, and because there is no monitoring of other source inputs into the Ala Wai Canal, the Manoa-Palolo stream gauge data was increased by 30% to account for the other missing inputs, including drainage canals, surface runoff, etc.

2.2 *Biological Model*

For this study, we use a biological model to examine the role of light in the time evolution of *Enterococcus* spp. coupled as a tracer in the hydrodynamic model. The biological model is based upon the ultra-violet (UV) decay model from Hassen et al., (2000):

$$\frac{dN}{dt} = -kIN, \tag{1}$$

where k ($m^2\ W^{-1} day^{-1}$) is the UV inactivation coefficient for *Enterococcus* spp., I is the intensity of UV irradiation ($W\ m^{-2}$), and N is the concentration of *Enterococcus* spp. ($nmol\ m^{-3}$). k is strain-specific, and bacteria resistant to UV irradiance are characterized by low k. We choose k equal to that detailed in Davies-Colley et al., (1994) who found that only 10% *Enterococcus* spp. is viable after 81 minute exposure from experiments with mid-day irradiances of $1200\ W\ m^{-2}$.

As *Enterococcus* spp. distributions are not restricted to the surface layer, we must determine the average diffuse attenuation coefficient, a in m^{-1}, for UV penetration in coastal tropical waters for Mamala Bay. The UV (280-420 nm wavelength) irradiance in water decays exponentially with depth:

$$\frac{dI}{dz} = -aI_d, \tag{2}$$

where I_d is the downwelling UV irradiance at depth z and a is the spectral attenuation coefficient (Parsons et al., 1977). Connolly et al., (1999) computed the attenuation coefficient at the 10 m isobath in Mamala Bay and found an average decay rate of 0.212 m^{-1}. UV irradiance is the primary spectral band that causes inactivation (loss of culturability) in bacteria, but makes up less than 10% of the total solar irradiance.

Blue light (475 nm) is the photoreactivation band which accounts for 0.5% of the total solar radiation (Hassen et al., 2000). Photoreactivation is the ability of micro-organisms to repair UV damaged DNA. Using (2), we attenuate the amount of blue light at depth. The full biological model with reactivation is given by:

$$\frac{dN}{dt} = -kIN + pIN, \quad (3)$$

where p is the growth coefficient due to photoreactivation.

Initially, *Enterococcus* spp. was used as a passive tracer with the biological decay model disabled in order to determine the effects of the physical forcing from ambient flow, wind, tides, and waves. We identify the plume by waters that meet or exceed a single-sample maximum of 100 CFU of *Enterococcus* 100 mL^{-1} that is set as the threshold for acceptable water quality by Hawaii's Department of Health.

3. Results and Discussion

3.1 *Effects of Forcing*

We performed a detailed analysis of five outflow events and present two illustrative plumes (Table 2). Event 1 occurred on 11 December, 2008 at 10:00 HST. The model stream gauge recorded a peak streamflow of 101.5 $m^3 s^{-1}$ (recall model stream-flow was increased by 30% of observed). In the model, this caused an outflow event from the Ala Wai Canal with a peak ocean discharge around 12:00 HST. This was followed by a second peak streamflow of 46.8 $m^3 s^{-1}$ on the evening of 13 December that caused a continual modeled plume until the morning of 16 December. During Event 1 there were strong Kona winds that blew from the southeast to the northwest with an average speed of 6.14 m s^{-1} ± 1.95, and the peak model discharge occurred during spring tide with tidal amplitudes near 70 cm.

We compared this event with Event 2 on 25 October, 2005 at 01:00 HST, the model stream gauge recorded a peak streamflow of 125.5 $m^3 s^{-1}$ that was preceded by a small event (90% smaller) two days earlier. Both rain events caused a continual outflow to occur from the Ala Wai Canal with a modeled peak ocean discharge on 25 October at 01:00 HST. The model plume began to flow out of the Ala Wai Canal on 23 October at 08:00 HST and lasted until the evening of the 26th. Modeled Trade winds had a mean speed of 5.11 m s^{-1} ± 1.36, and the maximum outflow was during a neap tide with an amplitude of approximately 30 cm.

For both Event 1 and Event 2, the plume experienced the greatest surface area for the ambient (NOFRC) and tidal forcing (TFRC) cases (Figure 3). For Event 1, mean near-shore circulation was to the east with magnitudes ranging from 10-20 cm s^{-1} by the Ala Wai Canal causing most of the plume to flow to the east; however, some of the plume dispersed both offshore and to the west (Figure 4a). For Event 2, the small outflow preceding the primary discharge combined with a mean circulation to the west spreading the plume across the surface (Figure 4d). Tidal forcing caused the plume to oscillate alongshore to the east on an ebb tide and to the west on a flood tide, which also resulted in the plume having a large surface area for both events. Surface areas were reduced for the wind forcing (WFRC) and maximum wave forcing (MFRC) experiments. For these comparisons, the differences between the MFRC and average wave forcing

(AFRC) experiments were not significant, and we will focus on the MFRC results. In response to the direction of the waves and the mixing that occurred, the surface area of the MFRC plume was reduced by 41% for Event 1 and 75% for Event 2 compared to the NOFRC case. For the WFRC experiments surface areas were reduced by 31% for Event 1 and 85% for Event 2 (Figure 3).

Because the discharges are caused by aperiodic rain events, the plume is freshwater with a typical modeled salinity of 2. Tomlinson et al. (2011) observed similar salinities in the surface waters of the Ala Wai Canal during rain events. For both events, the modeled plume reached maximum depths of approximately 1 m for the NOFRC and TFRC cases because neither the ambient flow or tidal forcing were able to overcome the density stratification of the freshwater lens to mix the plume deeper (Figure 5). The magnitude of the wind caused the plume to mix to greater depths for Event 1 (Figure 5a). Kona wind speeds began increasing the morning of 10 December and reached 10.3 m s^{-1} by late on 11 December causing the plume to be forced onshore and to the west extending past Sand Island into a deep lagoon where it mixed to depths of 4.4 m. For Event 2, the depth of the plume was not increased for the WFRC case compared to the NOFRC case because of a lower peak wind speed of 6.2 m s^{-1} (Figure 5b). Plumes reached the greatest depths for experiments with wave forcing. For Event 1, the mean circulation remained to the east with wave forcing, which forced the plume onto Waikiki beaches (Figure 4c). Increased significant wave height was found in the model within the Waikiki bight showing that waves propagating from the south-southwest break upon entering the Waikiki bight causing the plume to mix to maximum depths of 5.5 m. For Event 2, the mean circulation remained to the west forcing the plume towards Ala Moana Beach Park (Figure 4f). Wave forcing mixed the plume to depths of almost 4.5 m in the deep swimming area fronting the park. It is important to consider the depth of the plume because *Enterococcus* spp. may persist longer at depths where UV irradiation does not penetrate.

To help understand the temporal evolution of the plume mass, we examined the transport of *Enterococcus* spp. out of the canal in both alongshore and cross-shore directions. We created a western transect 1200 m to the west of the discharge mouth and an eastern transect 1200 m east with both transects extending from the shore to 800 m

offshore. A third transect connects east and west to measure the cross-shore transport. The *Enterococcus* spp. transport V_{entero} is calculated using (adapted from Choi and Wilkin, 2007):

$$V_{entero} = \iint_{-H}^{\eta} \left(1 - \left(\frac{E_o - E}{E_o}\right)\right) u \, dz \, dx, \qquad (4)$$

where η is the sea surface height anomaly, H is depth, E_o is the background *Enterococcus* spp. concentration used for the Manoa stream (150 nmol m^{-3}), E is local *Enterococcus* spp. concentration, u is the horizontal velocity normal to the transect, and integrated across the vertical section. The sum of transport across each section was computed over a 24 hour period for each event to account for diurnal and semidiurnal tides (when tides were included).

For Event 1, 73% of the total transport for the NOFRC experiment went offshore, as compared to only 8% for the WFRC case (Figure 6a). Without the wind, the plume moved almost completely offshore (as determined by the transect 800 m offshore) helping to separate itself from recreational beaches; however, when the onshore Kona winds were present, the plume persisted for five days along the beaches. The wind played an important role in the cross-shore advection of the plume because it forced the *Enterococcus* laden plume onshore (Figure 4b). Trade winds were dominant during Event 2 and did not cause an increase in the offshore transport as it comprised approximately 60% of the total transport for the NOFRC and WFRC experiments (Figure 6b). For MFRC experiments, offshore transport comprised 50% for Event 2 and almost 85% for Event 1.

The transport of *Enterococcus* spp. was increased across the western section for experiments with wind and/or wave forcing (Figures 7 and 8). For Event 1, the transport across the western section for the NOFRC experiment comprised 3% of the total transport, compared to 76% with Kona winds from the southeast forcing the plume to the northwest (Figure 7b). The westward transport was increased by 7% for the MFRC case compared to the NOFRC case for Event 1. For Event 2, the plume stayed to the west of the mouth of the Ala Wai Canal due to the direction and magnitude of the Trade winds and waves (Figure 4e and f). Due to the strong easterly component of the Trade winds, there was no eastern transport for the WFRC experiment and 2% for the MFRC

experiment compared to 15% for the NOFRC experiment (Figure 8a). Transport across the western section made up 25% of the total transport for the NOFRC case, 40% for the WFRC case, and 50% for the MFRC case (Figure 8b). To the east of the mouth of the canal there is shallow reef causing the incoming waves to pile water in this region. Once the water has piled in this region, the plume flushes to the west increasing the amount of westward transport for experiments with wave forcing (Figure 4c and f).

To quantify the effects of the physical forcing on the plume, we examined the individual contributions to the momentum equation. Results shown are for a 24 hour time average around the peak outflow. For cross-shore momentum balance terms, positive is onshore and negative is offshore. For alongshore momentum balance terms, positive is to the east and negative is to the west.

Vertical sections of the cross-shore momentum balance terms were analyzed for an alongshore transect. Since the Trade winds began blowing on the 23rd of October and persisted for more than two days for Event 2, the plume experienced an Ekman forcing with a positive Coriolis force causing a 15 cm s^{-1} increase in the westward alongshore current (Figure 9). For Event 1, Kona winds were variable and did not persist for more than two days; therefore, the alongshore current did not experience an increase due to Ekman forcing.

To further examine the mixing of the plume by wind and/or wave forcing, vertical sections along a cross-shore transect for alongshore momentum balance terms were analyzed. The vertical advection for both events was weak for experiments without wave forcing within the upper 2 m; however, with wave forcing the vertical advection was over twice as strong up to 5 m deep. Although Kona winds caused mixing of the plume within a deep lagoon, the majority of the plume was constrained within the first two meters for experiments with wind forcing.

Because the majority of the plume remained near the surface, we examined depth-integrated momentum balance terms for the upper 2 m. The cross-shore momentum balance terms for both events along a cross-shore transect that extends from 200 m within the Ala Wai Canal to 1200 m offshore were examined. For the Event 1 WFRC experiment, Kona winds created an onshore wind force balanced by an offshore pressure gradient (Figure 10a). For Event 2 WFRC, the offshore wind force due to Trade winds

was balanced by a positive Coriolis force (Figure 10b). For the MFRC experiments for both events an onshore pressure gradient was balanced by an offshore surface radiation force.

Alongshore momentum balance terms were analyzed for a transect that extends approximately 2000 m to the west of the mouth of the Ala Wai Canal and 1000 m to the east. For both events, due to the additional mass of freshwater near the mouth of the Ala Wai Canal, a pressure gradient anomaly was set up such that to the west of the mouth the pressure gradient force was to the west, and to the east of the mouth the pressure gradient force was to the east (Figure 11). For Event 2, the strong westerly component of the Trade winds overcame the easterly pressure gradient dispersing the plume to the west of the mouth of the Ala Wai towards Ala Moana Beach Park (Figure 11b). The variable Kona winds were not able to overcome the easterly pressure gradient allowing some of the plume to disperse both to the west and the east (Figure 11a). MFRC experiments experienced a balance between the pressure gradient, radiation force, and bottom stress in the alongshore momentum balance.

Collectively over the five modeled events, surface area patterns were similar in that NOFRC and TFRC cases experienced the largest surface areas and were decreased for the WFRC and MFRC cases. The maximum depth of the plume was the greatest for all events with maximum wave forcing. Offshore transport was decreased for events with Kona winds and westward transport was increased for events with Trade winds. In the cross-shore momentum balance for events with Kona winds, the onshore wind component was balanced by an offshore pressure gradient. For events with Trade winds, the offshore wind force was balanced by a positive Coriolis force. In the alongshore momentum balance, the increased sea surface height at the mouth of the Ala Wai Canal was balanced by a westerly pressure gradient to the west of the mouth of the Ala Wai Canal and an easterly pressure gradient to the east of the mouth.

3.2 *Light Effects on Plume*

We now utilize the fully coupled model with all physical forcing and the *Enterococcus* biological model to investigate the fate of the harmful bacteria within the plume itself and to predict how physical forcing and light influences the extent and duration of harmful bacteria contained in the plume. For this study, we examined the

plume of *Enterococcus* spp. contaminated waters from the Ala Wai Canal for five different rain events that occurred during 2005-2009 and compared modeled concentrations to local water quality measurements. Water quality samples were collected by the City and County of Honolulu during or shortly after each of the five events. Three shoreline stations shown on Figure 1 Ala Moana (AM), Magic Island (MI), and Waikiki (WK) and four offshore stations (C1, C2, C3, C4) were chosen to compare with model data. Water quality samples are taken at the surface so model output was also taken at the surface for cases WTFRC, WTAFRC, and WTMFRC (abbreviations defined in Table 1).

First we compared modeled *Enterococcus* spp. concentrations with and without inactivation from solar radiation at shoreline stations for both events. UV irradiation inactivates *Enterococcus* spp. causing a significant decrease in concentration. For Event 1, maximum concentrations occurred during the afternoon on 11 December with a peak outflow in the morning allowing UV inactivation to begin earlier than seen for Event 2 (Figure 12). *Enterococcus* spp. concentrations were reduced by approximately 50% at stations WK and MI and by 30% at station AM when considering UV inactivation; however, concentrations were still three times above the limit at all stations for the three cases. For the WTFRC and WTMFRC cases at station WK, concentrations were above the limit for four hours, then dropped below the limit for four hours, and then exceeded the limit again due to tidal oscillations. Four hours later concentrations were below the health advisory limit for the WTMFRC case, and eight hours later for the WTFRC case. For the WTAFRC case, concentrations were over the limit for 16 hours at station WK; therefore, the combination of tidal oscillations, Kona winds, and average southwest swell conditions resulted in *Enterococcus* spp. concentrations exceeding water quality standards.

Modeled *Enterococcus* spp. concentrations were above the health advisory limit for stations to the west of the Ala Wai Canal (AM and MI) immediately following the peak outflow for all cases as a result of Kona winds, a flood tide, and waves forcing the plume to the west. Station AM is farther west than MI, so concentrations were above the limit two hours after the peak streamflow; whereas, concentrations were above the limit at station MI immediately following the peak streamflow. For both stations, AM and MI,

concentrations reached a peak in the afternoon on 11 December for all cases, decreased due to inactivation, and began increasing at night as continual streamflow added *Enterococcus* spp., reaching maximum concentrations during the early morning of 12 December (Figure 12a). Concentrations remained above the limit for 14 hours on 12 December for station MI for the WTFRC case and ten hours for the WTAFRC and WTMFRC cases. At station AM, concentrations were above the limit for 12 hours for the WTFRC and WTAFRC cases, and for eight hours for the WTMFRC case. When surface waves were included in the model, the amount of time *Enterococcus* spp. concentrations remained above the health advisory limit was reduced.

The peak outflow for Event 2 occurred at night with maximum *Enterococcus* spp. concentrations early the following morning for all stations. Because the peak outflow occurred in the absence of solar radiation, maximum concentrations were initially similar for model runs with and without UV inactivation (Figure 12b). Without waves, concentrations remained below the health advisory for all stations. As a result of vertical mixing when including waves, *Enterococcus* spp. concentrations were above the threshold for almost all stations because UV inactivation of *Enterococcus* spp. was reduced. Model concentrations surpassed the threshold at all stations beginning early in the morning for the WTAFRC case and remained above the threshold for six hours. For the WTMFRC case, maximum model *Enterococcus* spp. concentrations occurred one (MI) to three (AM) hours after the outflow began and were three times above the limit. Six hours later, concentrations decreased and were below the limit. Concentrations remained below the limit at station WK because waves forced the plume to the west away from the station.

Modeled *Enterococcus* spp. concentrations may not fully represent observed concentrations for four primary reasons. First, the background concentration of *Enterococcus* spp. in Manoa Stream was set as a constant based on few samples that have been taken; however, concentrations can vary particularly as a result of "first-flush effects" (discussed later). Second, the attenuation coefficient was measured in tropical seawater, not a turbid freshwater plume like that flowing out of the Ala Wai Canal. Thus, modeled UV irradiation was able to penetrate deeper into the plume, causing concentrations to be lower in the model versus observational data. Third, non-point

source surface runoff into Mamala Bay likely contributed to *Enterococcus* spp. abundance not accounted for in the model. Fourth, we did not model actual wave conditions for each event, relying upon the characteristic average and maximum waves.

The covariance among all seven shoreline and offshore stations was computed for each event using modeled *Enterococcus* spp. concentrations and using a six year time series of observed *Enterococcus* spp. concentrations (Figure 13). Covariance matrices for both modeled and observed data showed that there was similar behavior between shoreline stations; however, there was no covariance among shoreline and offshore stations. This suggests that the outflow from the Ala Wai Canal did not reach offshore stations and was constrained near-shore. Observed *Enterococcus* spp. concentrations at offshore stations showed evidence of contamination, which were likely from the Sand Island Outfall.

To evaluate the correlation between predicted (model) and observed (water quality) *Enterococcus* spp. concentrations, scatter plots were made. Significance tests were defined by the 95% confidence interval threshold unless otherwise noted. Model fits were performed on all available water quality data against corresponding model results (via linear time and space interpolation). Closed circles represent predicted values with concentrations below the observed assay detection limit of 1 CFU 100 mL^{-1} and open circles represent predicted values above the assay limit. For shoreline stations we found that the model correlates well with the observed for predictions greater than the assay limit and correlates poorly with observed when below the limit. The model consistently underestimates concentrations below the assay limit suggesting that there are other sources of water contamination when there is little to no outflow from the Ala Wai Canal. However during high outflow events, the Ala Wai effluence dominates the water quality. With all five outflow events and all shoreline stations included, the WTFRC case showed the highest correlation to observed *Enterococcus* spp. concentrations (R^2=0.1471), and when the WK station was removed the correlation improved (R^2=0.4531) (Figure 14). This suggests that contamination at the WK station is not from the Ala Wai Canal effluent plume, but from other non-point source runoff. For offshore stations, most concentrations fell below the assay detection limit, showing again that the Ala Wai plume is constrained near-shore.

Waves had the most significant effect on the persistence of *Enterococcus* spp. by minimizing UV inactivation. Observations at the Kilo Nalu Observatory, located approximately 2 km west of the Ala Wai Canal (Figure 1), showed a significant wave height of 3 m during Event 1 with a period of 9 s from 193^{o} that is similar to the modeled maximum swell conditions (WTMFRC). Water quality samples were collected at stations MI, AM, WK and in the Ala Wai Canal (AW) approximately 20 hours after the peak outflow occurred for Event 1. *Enterococcus* spp. concentrations sampled in the Ala Wai Canal were recorded as high as 2700 CFU 100 mL^{-1} even 20 hours after the event started and model values reached concentrations of 2500 CFU 100 mL^{-1}. For the WTFRC case, modeled *Enterococcus* spp. concentrations were low (89.3 and 52.7 CFU 100 mL^{-1}) for stations MI and WK and high for station AM (181.2 CFU 100 mL^{-1}) when compared to water quality data sampled on the morning of 12 December 2008. Model concentrations from the WTMFRC case were in agreement with water quality data at station MI and AM, but dropped off too quickly to compare well to station WK. Underestimates of concentrations at station WK are likely caused by non-point source surface runoff in this area.

The contribution of non-point source surface runoff to Mamala Bay depends on weather conditions prior to a rain event. During a period of low rainfall, *Enterococcus* may accumulate resulting in increased concentrations when mobilized by a rainfall event, a phenomenon known as "first-flush effect". Because the streamflow was below the mean base flow of 0.16 $m^3 s^{-1}$ prior to Event 1, a first-flush effect likely occurred (Tomlinson et al., 2011). This contributed to underestimates of *Enterococcus* spp. concentrations in the model. Because of the slightly increased streamflow that occurred two days before the peak streamflow, Event 2 did not experience a first-flush effect.

4. Conclusions

The physical forcing of ambient circulation, tides, winds, and surface waves affect the surface area, depth, direction, and distance offshore of the Ala Wai Canal discharge during rain events. The outflow from the Ala Wai Canal is a freshwater plume that is well-stratified as a surface lens and advected by the ambient circulation creating large surface areas. Tidal forcing does not cause significant mixing, allowing the plume to oscillate alongshore and offshore, and increasing the plume surface area. The outflow is affected by seasonal wind patterns with Trade winds dominating most of the year, but Kona winds may be present during the months of October-April. Trade winds force the Ala Wai outflow to the west, while Kona winds push the plume onshore and to the west. In the cross-shore momentum balance, Trade winds are balanced by the Coriolis force, whereas Kona winds are balanced by an offshore pressure gradient. Strong winds blowing during the beginning of an outflow event will mix the plume to greater depths. If there are south-southwest swell conditions during an outflow event from the Ala Wai Canal, the surface area of the plume will decrease because waves cause the plume to mix and stay near-shore. The depth at which the plume is mixed is significant as UV irradiation is the main cause of inactivation in *Enterococcus* spp. Mixing caused by wind and waves has a significant effect on sequestering *Enterococcus* spp. away from the light. Although the plume behavior between average and maximum wave forcing were minor, the effect of solar radiation amplified these differences.

Since there was no covariance between shoreline and offshore stations, model and water quality data showed that the combined forcings act to segregate near-shore water from offshore. The model well represented the plume from the Ala Wai Canal during rain events at shoreline stations; however, when there was no outflow the model poorly reflected observations, likely due to other sources of contamination.

Diagnostic models such as the one presented here are intended to complement traditional water quality sampling programs by offering enhanced spatial coverage and improved frequency. Water quality observations are essential public health faculties, although are limited by the number of sites monitored and time-lag of reporting results. Real-time predictive capabilities from ecosystem models may be invaluable to providing timely public health advisories.

5. References

Berdeal Garcia, I., B.M. Hickey and M. Kawase (2002) Influence of Wind Stress and Ambient Flow on a High Discharge River Plume. Journal of Geophysical Research, 107: 3130.

Choi, Byoung-Ju and J.L. Wilkin (2007) The Effect of Wind on the Dispersal of the Hudson River Plume. Journal of Physical Oceanography, 37: 1878-1897.

Connolly, J. P., A.F. Blumberg and J.D. Quadrini (1999) Modeling Fate of Pathogenic Organisms in Coastal Waters of Oahu, Hawaii. Journal of Environmental Engineering, 125: 398-406.

Davies-Colley, R.J., R.G. Bell and A.M. Donnison (1994) Sunlight Inactivation of Enterococci and Fecal Coliforms in Sewage Effluent Diluted in Seawater. Applied and Environmental Microbiology, 60: 2049-2058.

Egbert, Gary D., Andrew F. Bennett and Michael G.G. Foreman (1994) TOPEX/POSEIDON Tides estimated using a global inverse model. Journal of Geophysical Research, 99: 24,821-24,852.

Fairall, C.W., E.F. Bradley, D.P. Rogers, J.B. Edson and G.S. Young (1996) Bulk Parameterization of air-sea fluxes for Tropical Ocean-Global Atmosphere Coupled-Ocean Atmosphere Response Experiment. Journal of Geophysical Research, 101: 3747-3764.

Garvine, R.W. (1987) Estuary plumes and fronts in shelf waters: a layer model. Journal of Physical Oceanography, 17: 1877-1896.

Garvine, R.W. (1995) A dynamical system for classifying buoyant coastal discharges. Continental Shelf Research, 15: 1585-1596.

Guo, Xinya and A. Valle-Levinson (2007) Tidal effects on estuarine circulation and outflow Plume in the Chesapeake Bay. Continental Shelf Research, 27: 20-42.

Hamilton, P., J.J. Singer and E. Waddell (1995) Ocean current measurements, final report, Mamala Bay Study, project MB-6, Mamala Bay Study Comm., Honolulu, Hawaii.

Hassen, A., M. Mahrouk, H. Ouzari, M. Cherif, A. Boudabous and J.J. Damelincourt (2000) UV disinfection of treated wastewater in a large-scale pilot plant and inactivation of selected bacteria in a laboratory UV device. Biosource Technology, 74: 141-150.

Hickey, B.M., L.J. Pietrafesa, D.A. Jay and W.C. Boicourt (1998) The Columbia River Plume Study: Subtidal variability in the velocity and salinity fields. Journal of Geophysical Research, 103: 10,339-10,368.

Masse, A. K., and C. R. Murthy (1992) Analysis of the Niagara River plume dynamics. Journal of Geophysical Research, 97: 2403-2420.

O'Donnell, J. (1990) The formation and fate of a river plume: a numerical model. Journal of Physical Oceanography, 20: 551-569.

Orton, Philip M. and David A. Jay (2005) Observations at the tidal plume front of a high-volume river outflow. Geophysical Research Letters, 32:L11605.

Parsons, R.R., M. Takahashi and B. Hargrave (1977) Biological oceanographic processes. Pergamon.

Pullen, J.D. and J.S. Allen (2000) Modeling studies of the coastal circulation off Northern California: shelf response to a major Eel river flood event. Continental Shelf Research, 20: 2213-2238.

Shchepetkin, A.F. and J.C. McWilliams (2005) The Regional Ocean Modeling System: a split-explicit, free-surface, topography-following-coordinate ocean model. Ocean Modeling, 9: 347-404.

Venzon, N.C. Jr. (2007) Massive Discharge of Untreated Sewage into the Ala Wai Canal (Oahu, Hawaii): A Threat to Waikiki's Waters? Journal of Environmental Health, 70: 25-29.

Whitney, M.M. and R.W. Garvine (2006) Simulating the Delaware Bay buoyant outflow: Comparison with observations. Journal of Physical Oceanography, 36: 3-21.

Wiseman, W.J. and R.W. Garvine (1995) Plumes and Coastal Currents Near Large River Mouths Estuaries, 18:509-517.

Experiment Name	Wind Forcing	Tidal Forcing	Average Wave Forcing	Maximum Wave Forcing
NOFRC				
WFRC	X			
TFRC		X		
WTFRC	X	X		
AFRC			X	
WAFRC	X		X	
TAFRC		X	X	
WTAFRC	X	X	X	
MFRC				X
WMFRC	X			X
TMFRC		X		X
WTMFRC	X	X		X

Table 1. Experiment names for differing combinations of forcing. W designates Wind, T for tidal, A for average wave, and M for maximum wave forcing. NOFRC designates the ambient circulation without forcing.

Event Name	OCT05* (Event 2)	MAR06	NOV07	DEC08* (Event 1)	MAR09
Period: Start End	 10/16/05 11/1/05	 3/14/06 4/2/06	 10/29/07 11/12/07	 12/3/08 12/22/08	 3/6/09 3/23/09
Peak ($m^3 s^{-1}$) Streamflow: Date-Time:	 125.5 10/25-1am	 188.8 3/22-1am	 37.99 11/4-8am	 101.5 12/11-10am	 117.2 3/14-5am
Peak ($m^3 s^{-1}$) Plume Outflow: Date-Time:	 -55.56 10/25-2am	 -70.91 3/23-10pm	 -22.05 11/4-8am	 -72.16 12/11-12pm	 -44.15 3/14-6am
Wind (from) Direction	NE	S	E/NE	SE	E/NE
Average Wind Speed ($m s^{-1}$)	5.11	3.56	3.75	6.14	1.79
Tidal Amplitude (cm)	30	60	55	70	55
Mean Near-shore Flow Direction	East	West	East	East	West
Maximum Plume Area (m^2)	$1.5x10^7$	$3.2x10^7$	$9.1x10^6$	$9.0x10^6$	$1.87x10^7$
Maximum Plume Depth (m)	5	8	5	9	4

Table 2. Description and summary of conditions for five outflow events from the Ala Wai Canal. * events are presented in detail in the Results and Discussion section.

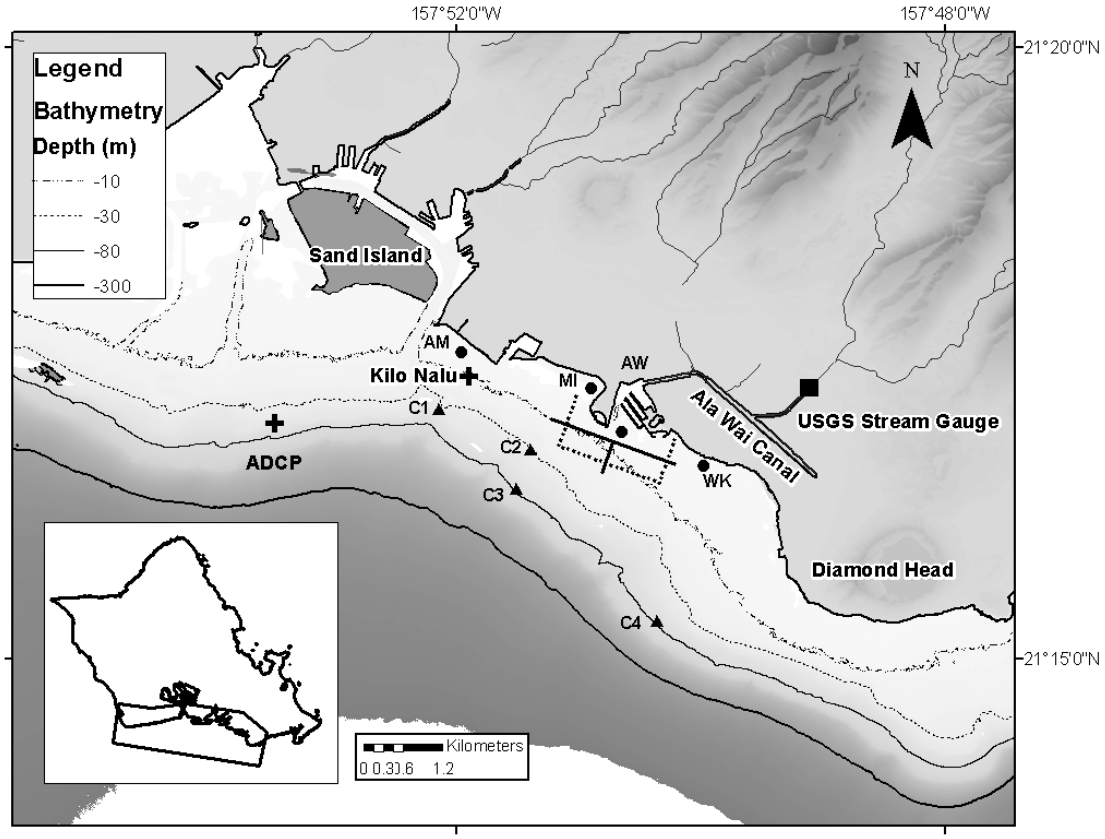

Figure 1. Map of study area including the Ala Wai Canal and water quality sampling stations. Black dotted lines are the locations of the *Enterococcus* spp. transport calculations. Black solid lines are the locations of the alongshore and cross-shore transects for the momentum balance calculations. Inset figure shows the island of Oahu and the box represents the model domain, which includes southern Oahu and Mamala Bay.

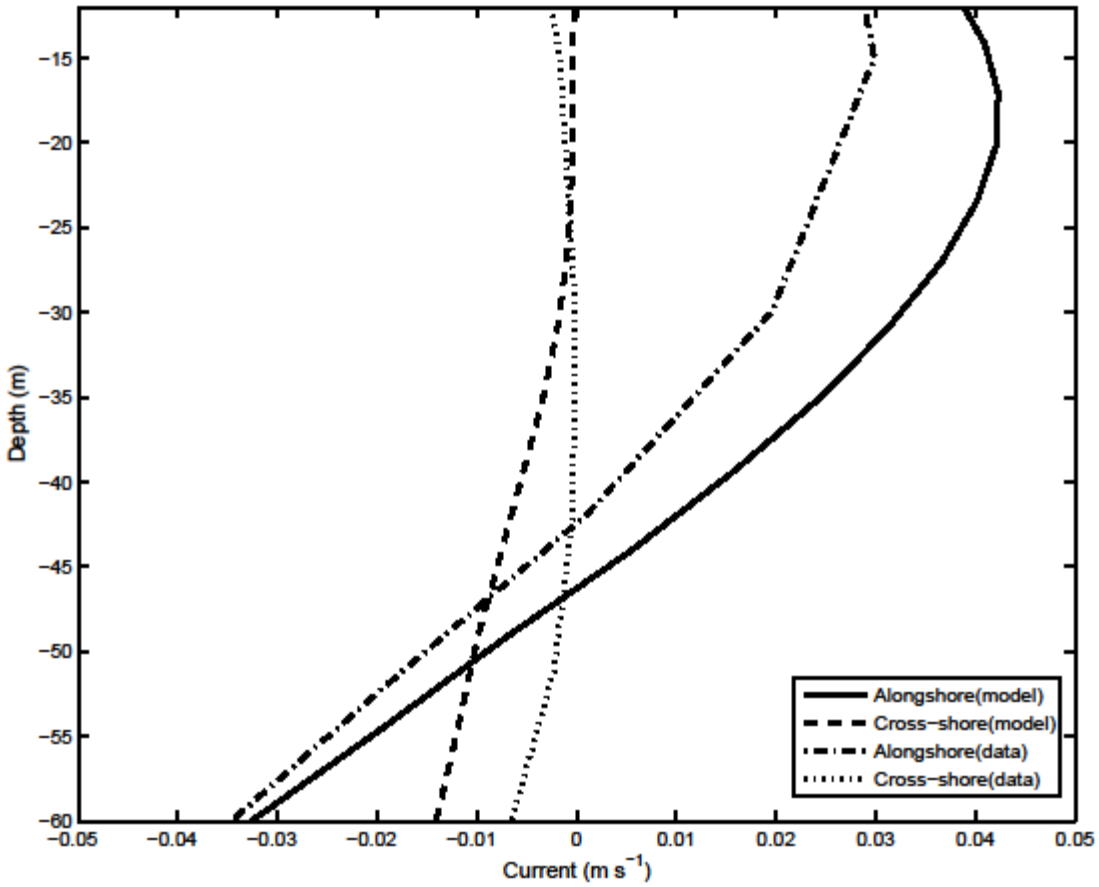

Figure 2. Mean currents of model output compared to ADCP data.

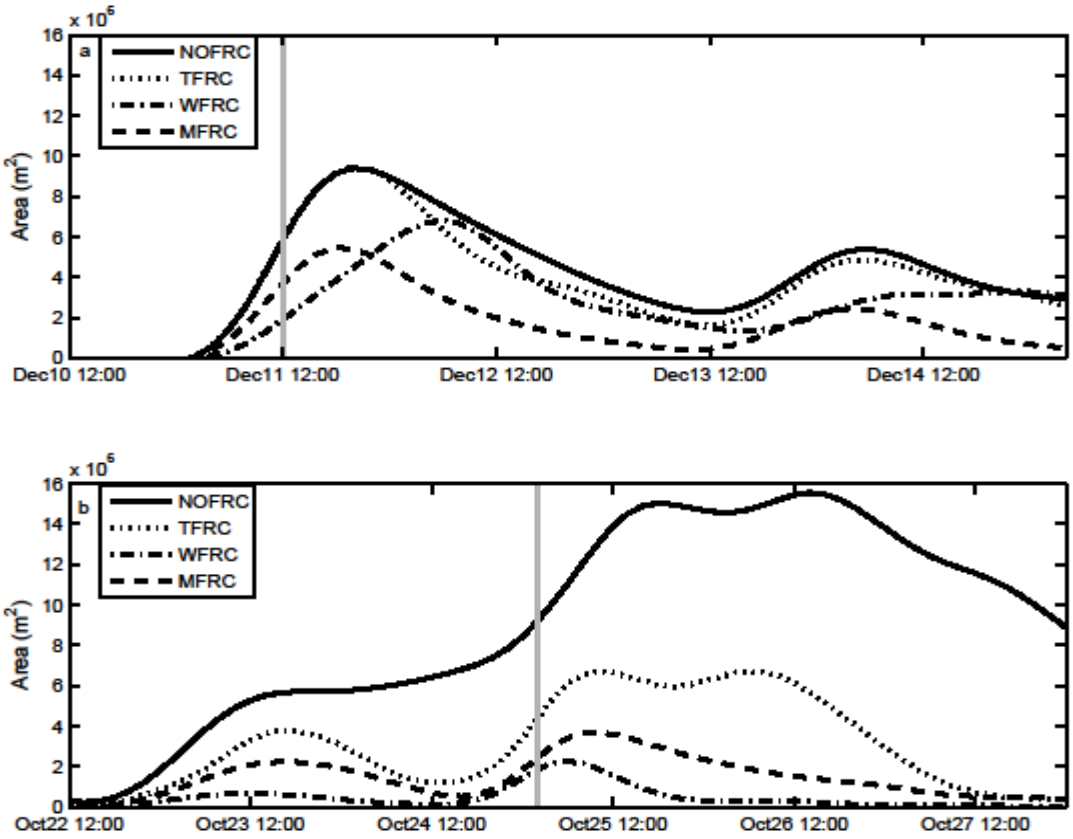

Figure 3. Surface area of plume above the health advisory limit for different model runs for Event 1 (a) and Event 2 (b). The gray line signifies when the peak outflow occurred from the mouth of the Ala Wai Canal. Date and time is in HST.

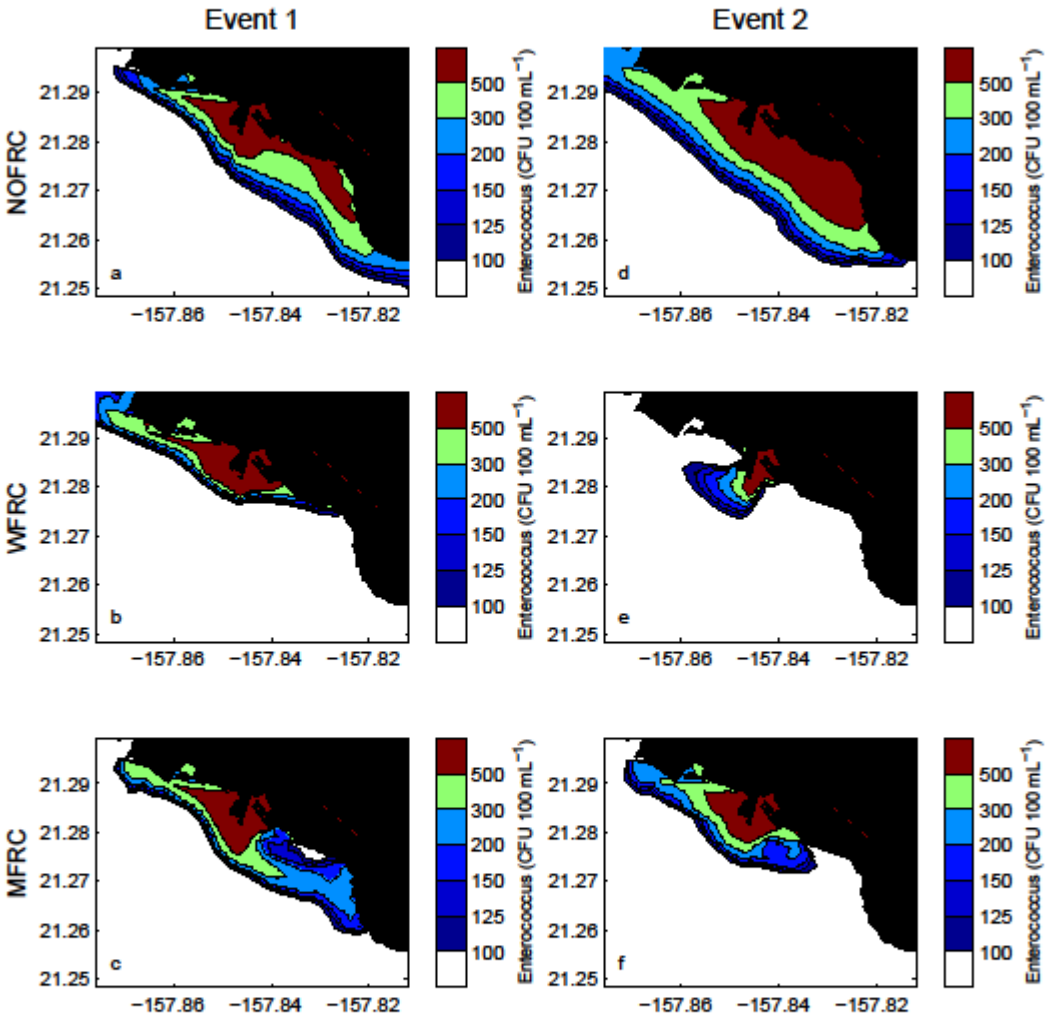

Figure 4. Effluent plume above health advisory limit for an average computed from when the peak outflow occurred until 24 hours later to show the general surface area and region the plume encompassed. Column 1 is Event 1; a is the NOFRC case, b is the WFRC case, and c is the MFRC case. Column 2 is Event 2; d is the NOFRC case, e is the WFRC case, and f is the MFRC case.

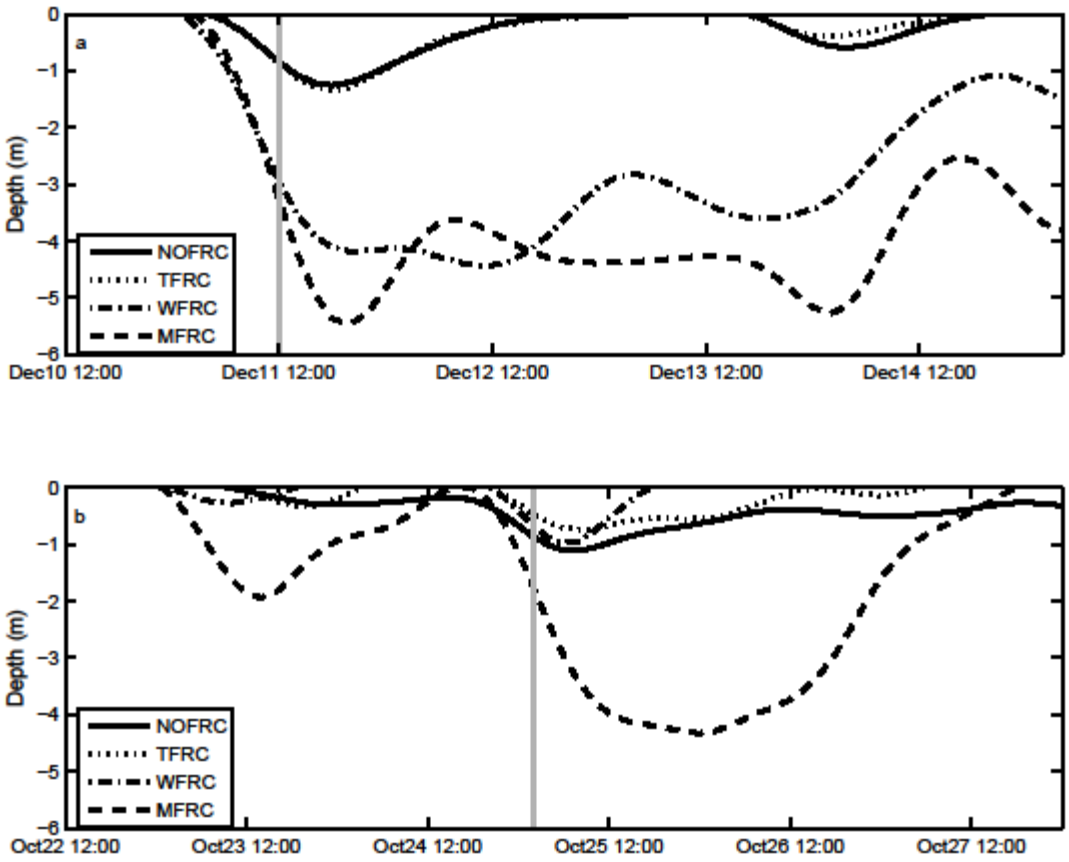

Figure 5. Maximum depth of plume above the health advisory limit for different model runs for Event 1 (a) and Event 2 (b). The gray line signifies when the peak outflow occurred from the mouth of the Ala Wai Canal. Date and time is in HST.

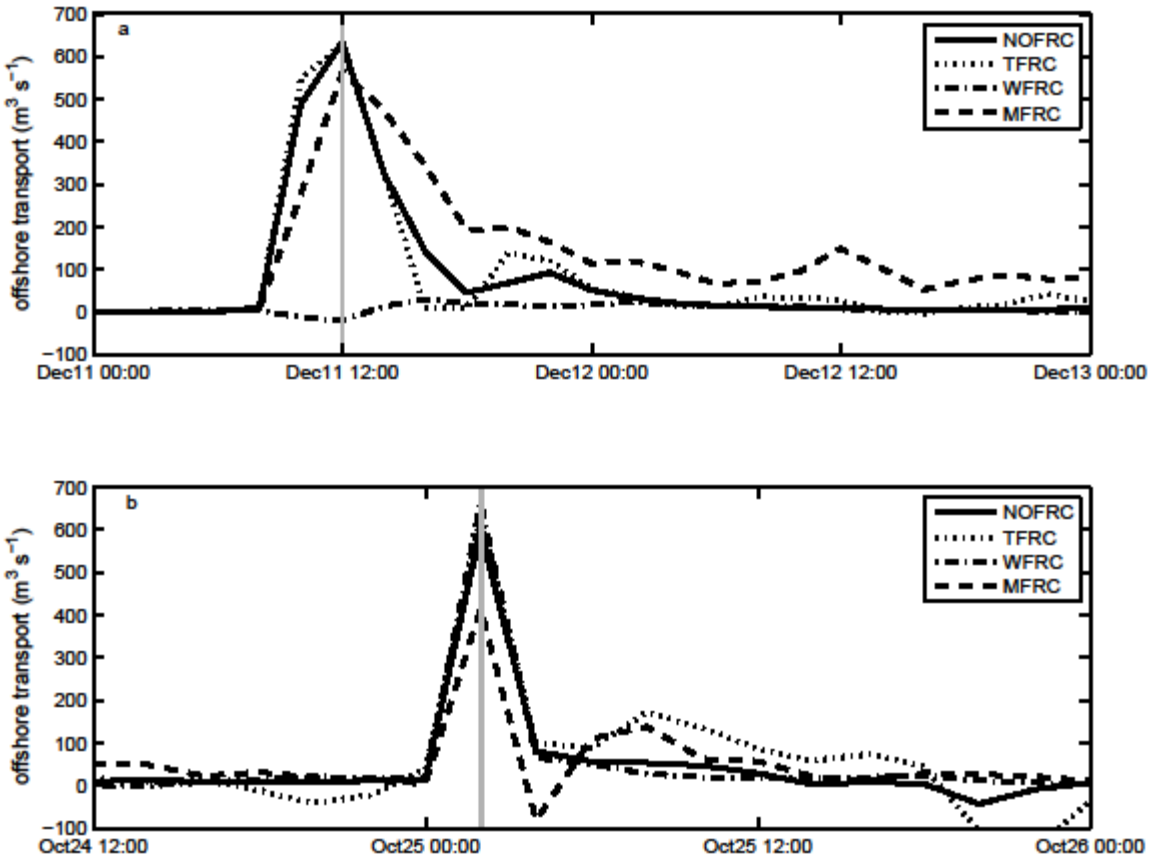

Figure 6. Transport of *Enterococcus* spp. above the health advisory limit where positive is to the south across the offshore transect for different model runs for Event 1 (a) and Event 2 (b). The gray line signifies when the peak outflow occurred from the mouth of the Ala Wai Canal. Date and time is in HST.

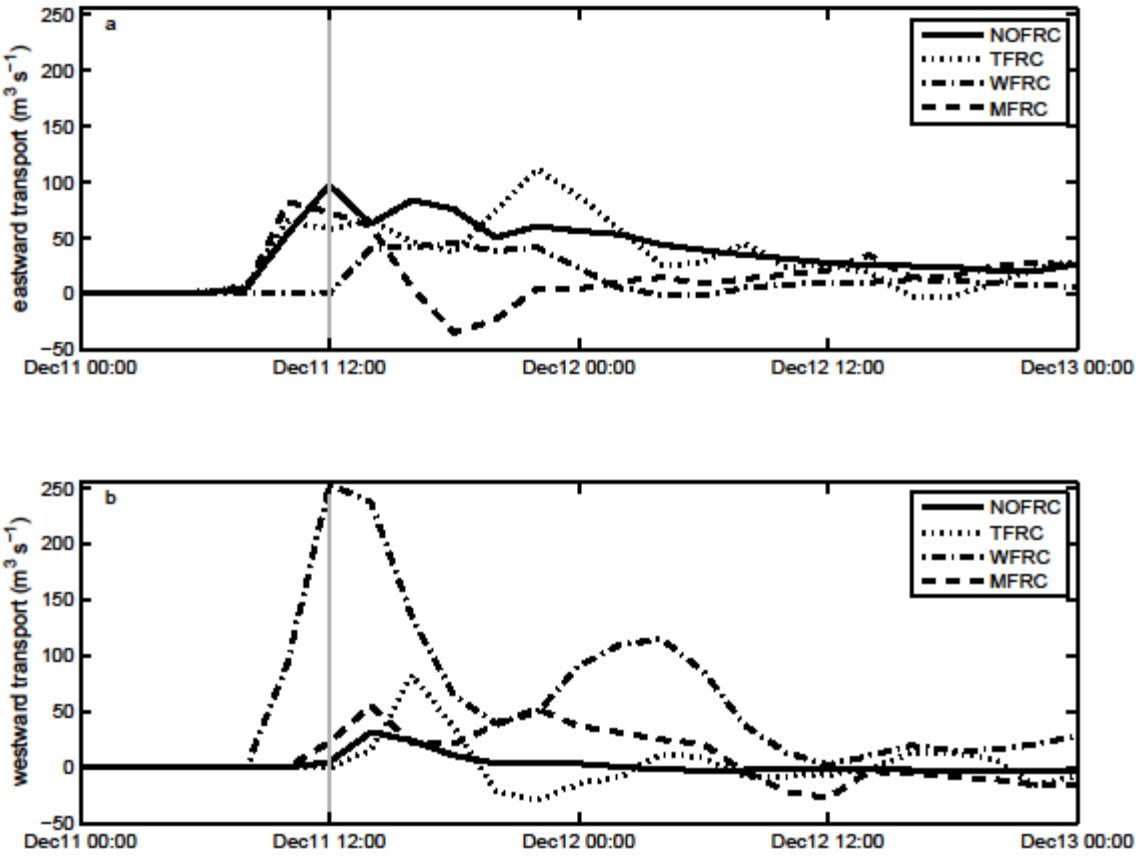

Figure 7. Event 1 transport of *Enterococcus* spp. above the health advisory limit for different model runs across eastern and western boundaries where transports flowing across each transect away from the mouth of the canal are positive. The gray line signifies when the peak outflow occurred from the mouth of the Ala Wai Canal. Date and time is in HST.

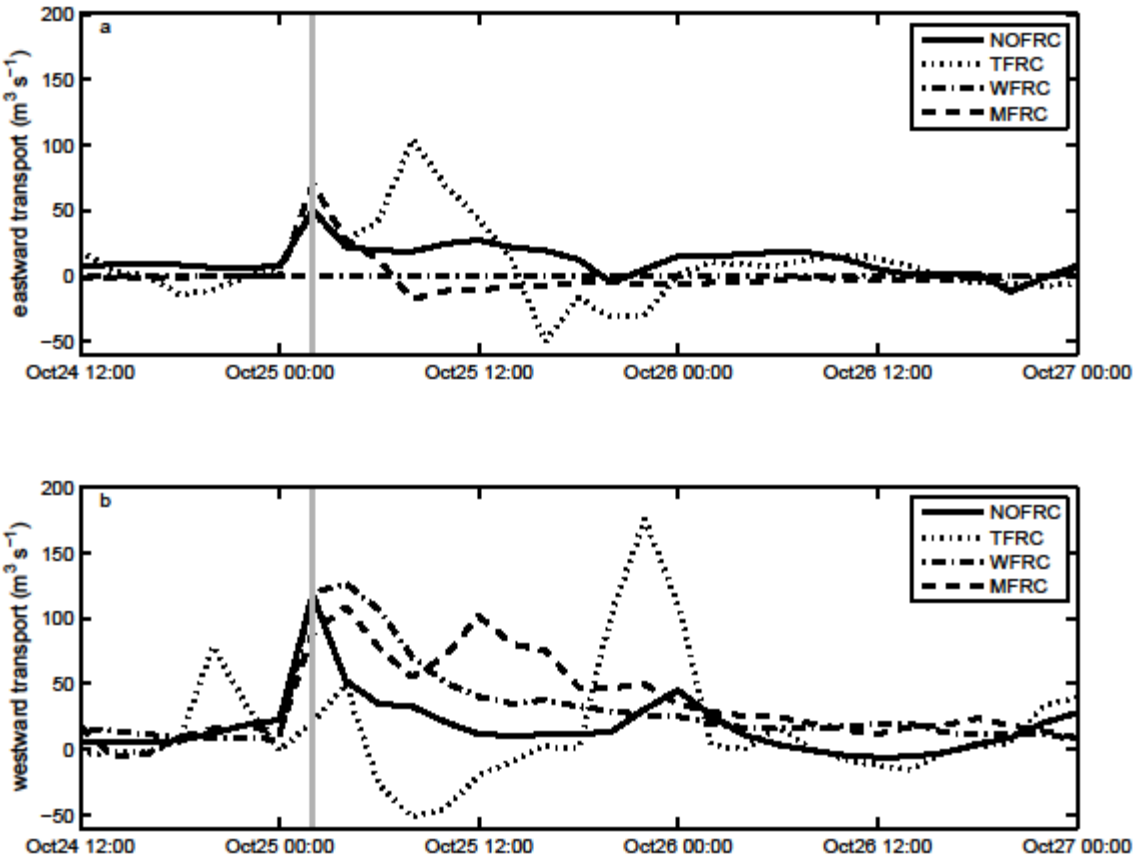

Figure 8. Event 2 transport of *Enterococcus* spp. above the health advisory limit for different model runs across eastern and western boundaries where transports flowing across each transect away from the mouth of the canal are positive. The gray line signifies when the peak outflow occurred from the mouth of the Ala Wai Canal. Date and time is in HST.

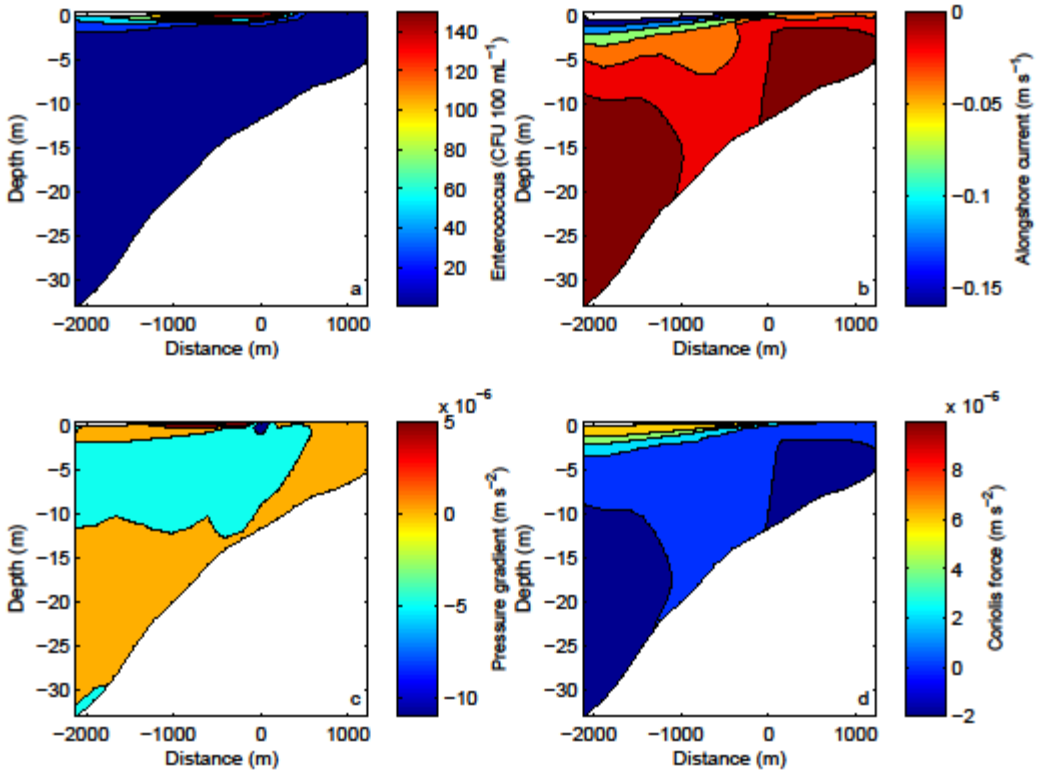

Figure 9. For Event 1 WFRC experiment, vertical structure for a 24 hour temporal mean the length of an alongshore transect where negative is to the west of the mouth of the Ala Wai Canal, located at zero, and positive is to the east of the mouth of: (a) *Enterococcus* spp., (b) the alongshore current, (c) the cross-shore pressure gradient force, and (d) the cross-shore Coriolis force.

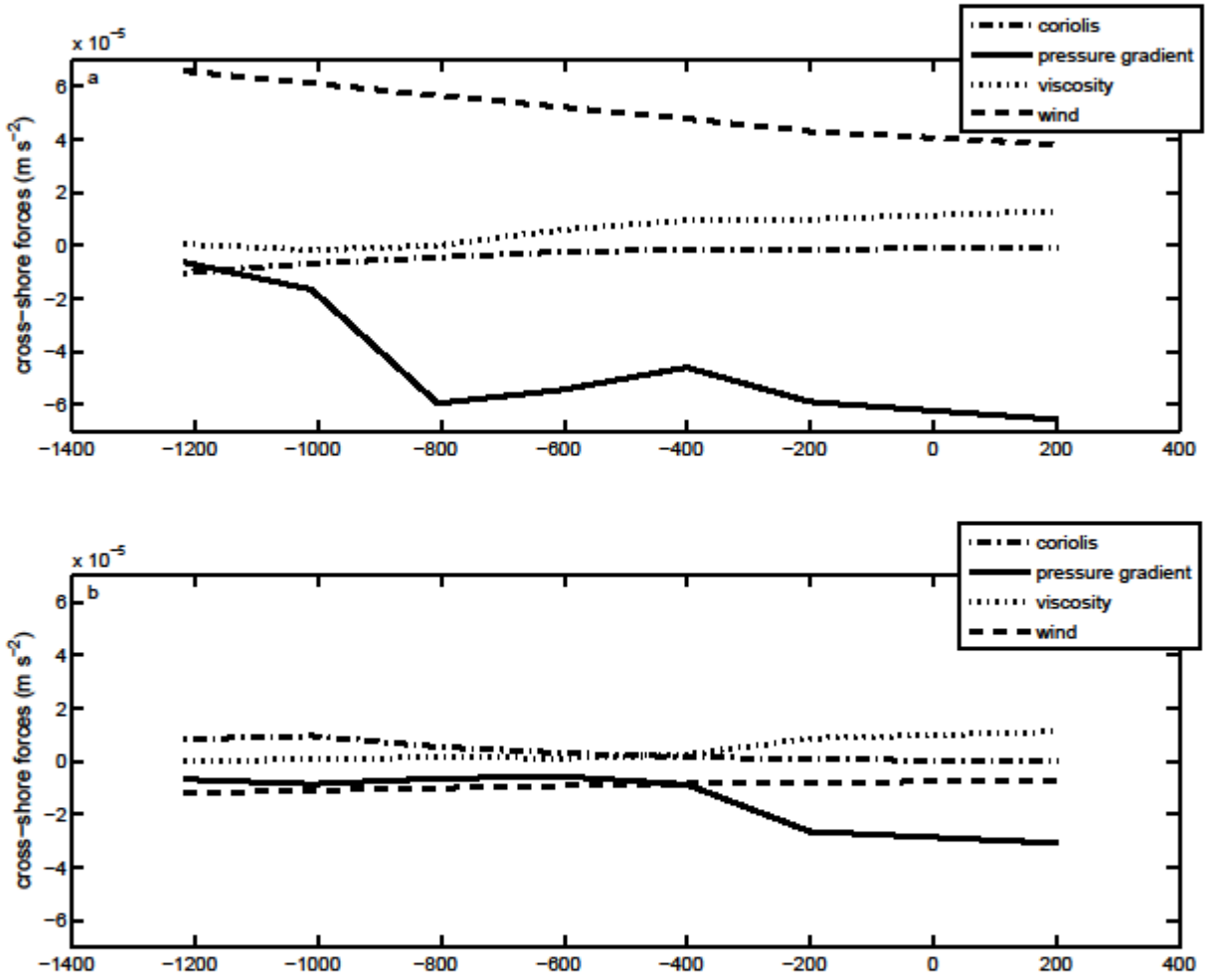

Figure 10. Depth-integrated for the upper 2 m cross-shore momentum balance forces for a 24 hour temporal mean the length of a cross-shore transect where negative is to the south of the mouth of the Ala Wai Canal, located at zero, and positive is to the north within the canal for the WFRC experiment for Event 1 (a) and Event 2 (b).

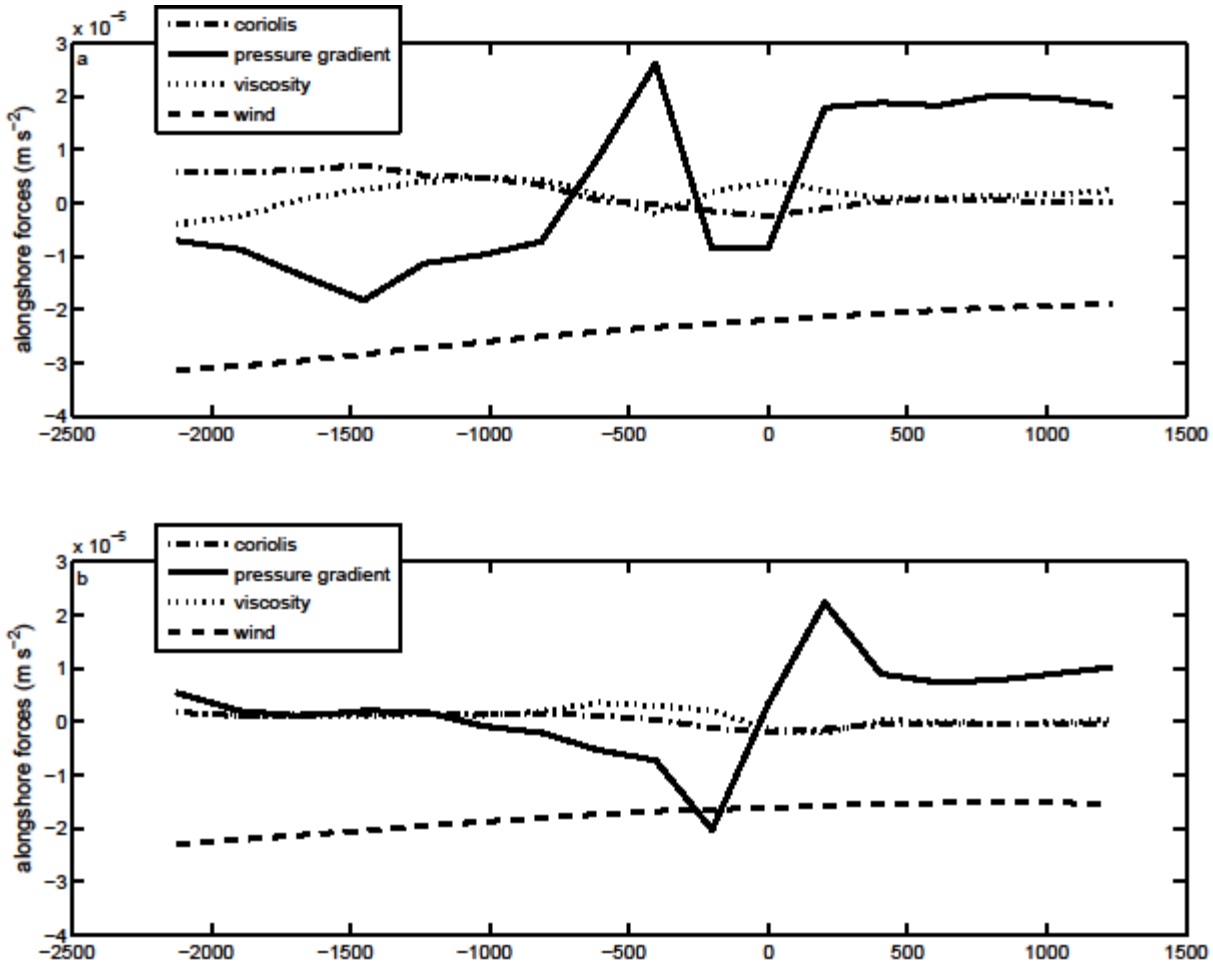

Figure 11. Depth-integrated for the upper 2 m alongshore momentum balance forces for a 24 hour temporal mean the length of an alongshore transect where negative is to the west of the mouth of the Ala Wai Canal, located at zero, and positive is to the east of the mouth for the WFRC experiment for Event 1 (a) and Event 2 (b).

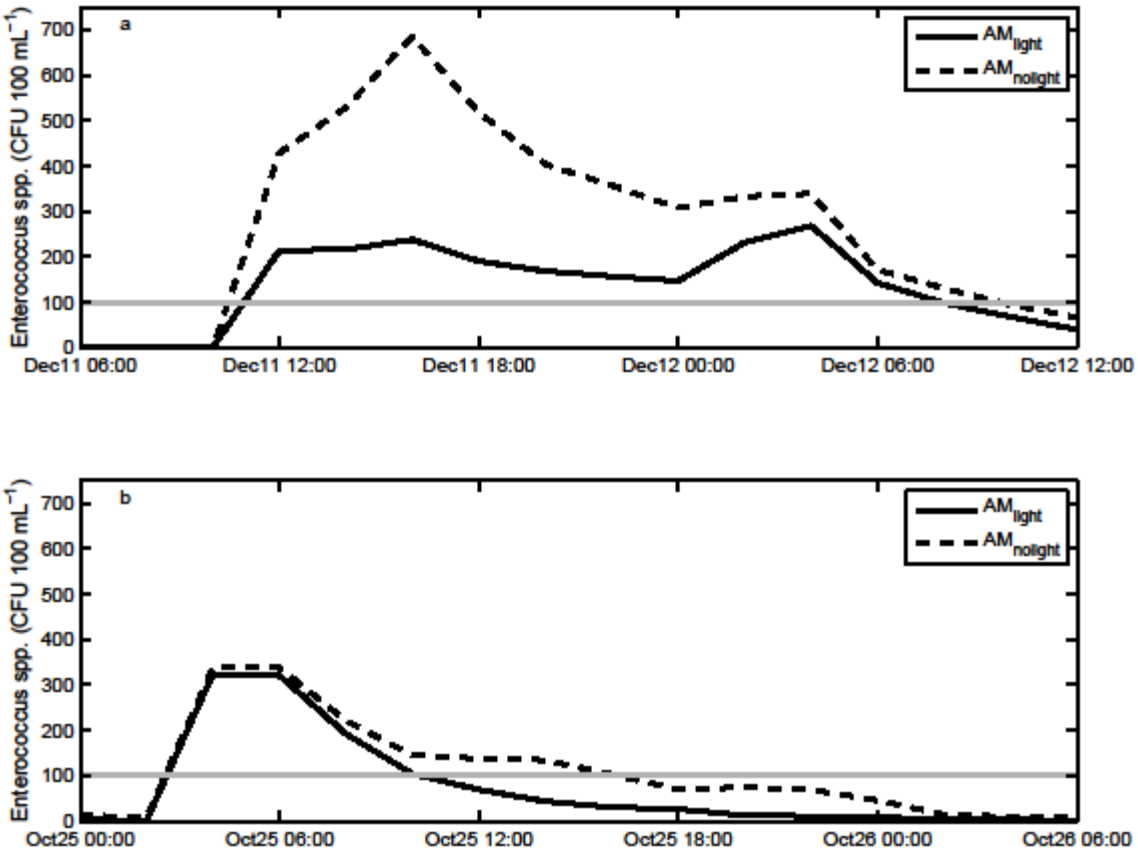

Figure 12. Non-inactivated (nolight) compared to inactivated (light) model *Enterococcus* spp. concentrations at station AM for the WTMFRC experiments for Event 1 (a) and Event 2 (b).

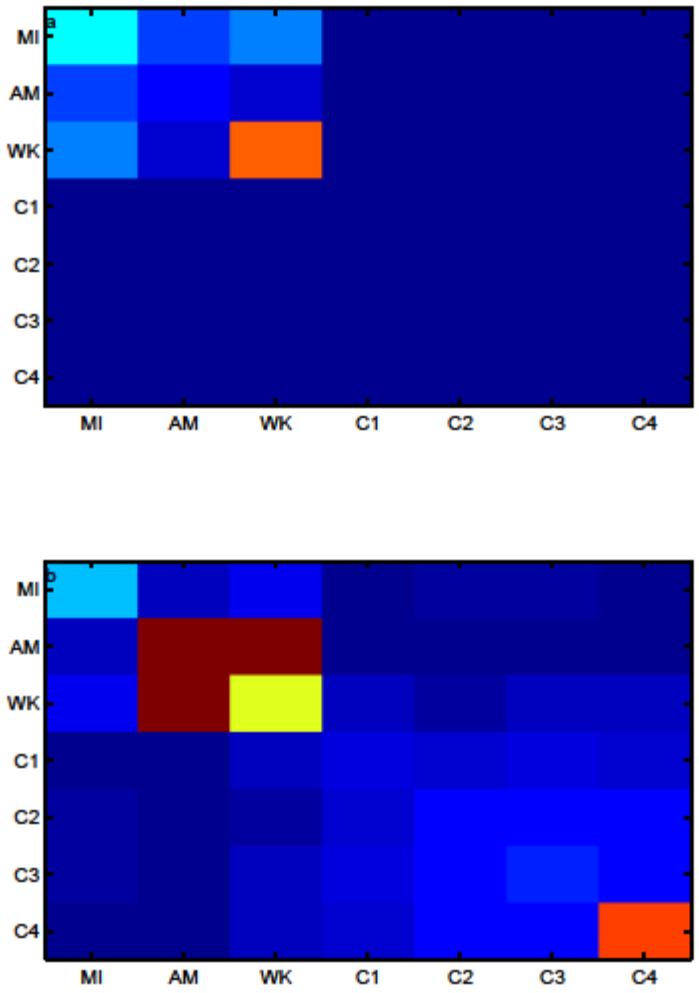

Figure 13. Covariance matrices for seven, shoreline (MI, AM, WK) and offshore (C1, C2, C3, C4), stations for modeled Event 1 WTFRC (a) and observed (b) *Enterococcus* spp. concentrations.

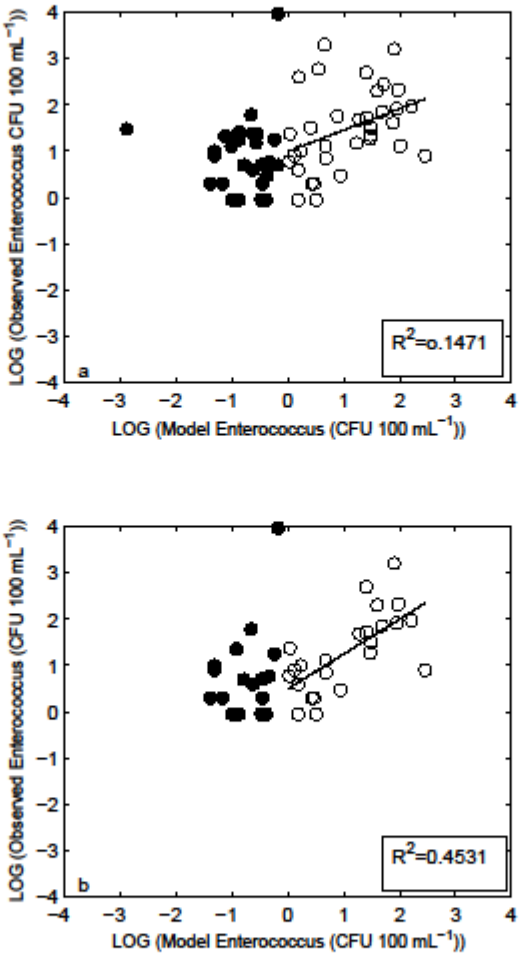

Figure 14. Scatter plots of modeled (x-axis) versus observed (y-axis) *Enterococcus* spp. concentrations for all five events for the WTFRC case for MI, AM, and WK stations (a) and for MI and AM stations (b). Closed circles represent predicted (model) values below the assay detection limit (1 CFU 100 mL^{-1}) and open circles represent predicted (model) values above the assay detection limit.